The Coastal Observation and Simulation with Topography (COAST) Experiment*

Nicholas A. Bond,[a] Clifford F. Mass,[b] Bradley F. Smull,[a,c] Robert A. Houze,[b] Ming-Jen Yang,[d] Brian A. Colle,[b] Scott A. Braun,[e] M. A. Shapiro,[f] Bradley R. Colman,[g] Paul J. Neiman,[f] James E. Overland,[h] William D. Neff,[f] and James D. Doyle[i]

ABSTRACT

The Coastal Observation and Simulation with Topography (COAST) program has examined the interaction of both steady-state and transient cool-season synoptic features, such as fronts and cyclones, with the coastal terrain of western North America. Its objectives include better understanding and forecasting of landfalling weather systems and, in particular, the modification and creation of mesoscale structures by coastal orography. In addition, COAST has placed considerable emphasis on the evaluation of mesoscale models in coastal terrain. These goals have been addressed through case studies of storm and frontal landfall along the Pacific Northwest coast using special field observations from a National Oceanic and Atmospheric Administration WP-3D research aircraft and simulations from high-resolution numerical models. The field work was conducted during December 1993 and December 1995. Active weather conditions encompassing a variety of synoptic situations were sampled. This article presents an overview of the program as well as highlights from a sample of completed and ongoing case studies.

1. Introduction

The Coastal Observation and Simulation with Topography (COAST) program has used intensive field observation and high-resolution numerical models to study the interaction of fronts and cyclones with the prominent coastal terrain of western North America. This issue of storm–coastal terrain interactions has been identified by the U.S. Weather Research Program as a research priority (Rotunno et al. 1996) and clearly is important for improving forecasts along mountainous coastlines.

While the West Coast has a generally benign climate, it can also have severe weather, often in association with landfalling cyclones and fronts. Notable recent examples include the heavy orographic precipitation and flooding in California's coastal zone that occurred during 9–10 January and 10–11 March 1995, and the strong winds (100+ mph) that buffeted the coast from central California to Washington during 11–12 December 1995 as an intense cyclone moved northward along the coast. These were extreme events, but more routine synoptic situations also produce topographically induced mesoscale features that can have considerable societal impacts.

The coastal mountains that extend along virtually the entire length of western North America represent a significant barrier to lower tropospheric flow. Their impact on the incident flow gives rise to a variety of mesoscale phenomena (e.g., barrier jets, orographically enhanced precipitation, and flow-splitting) within approximately 100 km of the coastline and substantially modifies the mesoscale structures of

[a]JISAO, University of Washington, Seattle, Washington.
[b]Department of Atmospheric Sciences, University of Washington, Seattle, Washington.
[c]NOAA/NSSL, Norman, Oklahoma.
[d]Central Weather Bureau, Taipei, Taiwan.
[e]NCAR, Boulder, Colorado.
[f]NOAA/ETL, Boulder, Colorado.
[g]National Weather Service, Seattle, Washington.
[h]NOAA/PMEL, Seattle, Washington.
[i]Naval Research Laboratory, Monterey, California.
In final form 21 March 1997.
Corresponding author address: Dr. N. A. Bond, NOAA/PMEL, 7600 Sand Point Way N.E., Seattle, WA 98115-0070.
E-mail: bond@pmel.noaa.gov
*NOAA/Pacific Marine Environmental Laboratory Contribution No. 1804 and Joint Institute for the Study of the Ocean and Atmosphere Contribution No. 421.

landfalling weather systems. Although these mesoscale coastal features greatly influence the weather of the coastal zone, they are not resolved adequately by the present observational network, and current operational numerical weather prediction (NWP) models lack the resolution to realistically simulate their evolution.

Comprehensive descriptions of the mesoscale flow around coastal orography are lacking, in particular for situations with significant evolution in the synoptic-scale flow. The central goal of the COAST field experiment has been to collect high-resolution observations from the coastal zone of the Pacific Northwest, particularly datasets that allow the description and modeling of mesoscale features produced and modified by orography.

The observational component of COAST relied principally on measurements taken by a National Oceanic and Atmospheric Administration (NOAA) WP-3D (P-3) research aircraft, supplemented by enhanced surface and upper-air measurements. These observations form the foundation for detailed case studies, which, in turn, have been used to validate simulations by high-resolution NWP models such as the The Pennsylvania State University–National Center for Atmospheric Research Mesoscale Model (MM5) and the Naval Research Laboratory's (NRL's) Coupled Ocean Atmosphere Mesoscale Prediction System (COAMPS) model.

The COAST experiment has been a joint program involving scientists from NOAA's Environmental Research Laboratories (ERL), the University of Washington, the National Weather Service (NWS), and NRL in Monterey. COAST received support from the Office of Naval Research (ONR) and NOAA, with additional assistance from the National Science Foundation. The ONR contribution came from an Accelerated Research Initiative on Coastal Meteorology; NOAA's involvement was through ERL, the Aircraft Operations Center, and the NWS.

This article presents some early results from COAST and is intended to illustrate some of the mesoscale phenomena of interest and the direction of research, rather than to summarize final results. Sections describing the scientific objectives and field operations set the stage for the main body of the paper, which consists of highlights from selected case studies. Some case studies have already been published (Overland and Bond 1995; Colle and Mass 1996) and many others are in progress. We were hoping to observe dramatic and significant coastal weather for our case studies; the glimpses presented here will show that this hope was realized.

2. Scientific issues

As noted above, the general goals of the COAST project have been to document and examine the interaction of the incident flow with the complex orography of the west coast of North America. The primary scientific issues being addressed by COAST include the following.

1) How are the nature, magnitude, and offshore extent of the orographic modification of the incoming flow determined by the characteristics of the topographical barrier and the incident flow (e.g., cross-barrier wind velocity and static stability)?
2) How are the mesoscale structures of fronts and cyclones modified as they approach and make landfall on coastal terrain? How are these modifications related to precipitation, cloud microphysics, and viscous effects in the coastal zone?
3) How well can high-resolution NWP model simulations duplicate the mesoscale atmospheric structures evident in coastal terrain? Are the mesoscale structures produced by the terrain so dominant that offshore mesoscale specification is unnecessary?

Many aspects of these issues have been addressed but generally for idealized situations or noncoastal environments. Theoretical studies (e.g., Smith 1981; Pierrehumbert and Wyman 1985; Smolarkiewicz and Rotunno 1989) have diagnosed the idealized nature of the orographic response as a function of nondimensional flow parameters such as the Froude and Rossby numbers. These results are consistent with observations of barrier jets (Parish 1982) and cold-air damming (Bell and Bosart 1988; Xu 1990) during steady-state flow. More typically, the orographic response is complicated because of its dependence on a combination of effects including variations in topography; temporal and spatial variations in the incident flow; diabatic, especially latent, heating; and viscous effects (e.g., Okland 1990). Most work on storm–terrain interactions involves orographic modification of fronts, particularly by the Alps, and includes theoretical (Blumen 1992; Gross 1994), modeling (Williams et al. 1992), and observational studies (Hoinka et al. 1990). Observational case studies of mesoscale storm phenomena along mountainous coasts (e.g.,

Mass and Ferber 1990; Overland and Bond 1993; Steenburgh and Mass 1996) have illustrated only a handful of events using limited datasets. The Cyclonic Extratropical Storms (CYCLES) project documented frontal precipitation structures along the Pacific Northwest coast (as reviewed by Houze 1991). CYCLES collected observations of changes in radar reflectivity as frontal rainbands moved onshore (e.g., Parsons and Hobbs 1983) but did not secure comprehensive documentation of the thermodynamic and kinematic fields accompanying these features.

The diagnosis of complicated situations such as the orographic modification of landfalling storms can often be done most effectively using high-resolution NWP models. The state-of-the-art mesoscale models are capable of realistically simulating the detailed structures of storms over the open ocean, as demonstrated by observational (e.g., Neiman and Shapiro 1993; Neiman et al. 1993) and numerical (e.g., Kuo et al. 1991; Grell and Shapiro 1994) case studies from the Experiment on Rapidly Intensifying Cyclones over the Atlantic. Such models hold the potential to simulate mesoscale storm structures in the coastal zone, but to date only limited datasets have been available for their validation.

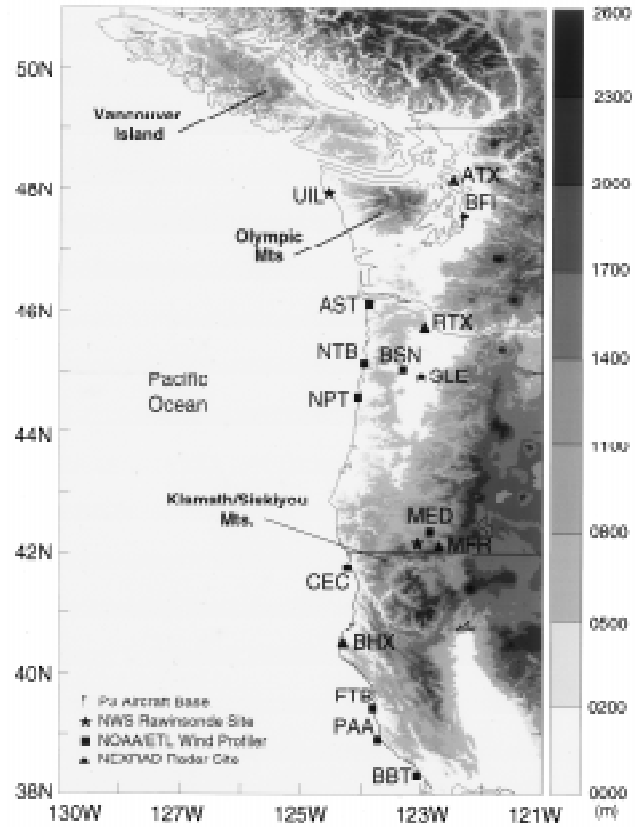

FIG. 1. Domain of the COAST field experiment. See figure key for explanation of symbols. Astoria, Oregon (AST), had the only wind profiler operating in 1993; all four sites had profilers operating in 1995.

3. Field operations summary

The two field phases of COAST were conducted in the Pacific Northwest during December 1993 and December 1995. A map of the study area (Fig. 1) reveals that the Pacific Northwest coast has a variety of terrain including prominent two-dimensional barriers on Vancouver Island and near the California–Oregon border (the Klamath–Siskiyou Mountains) and a nearly circular obstacle in Washington State (the Olympic Mountains). Figure 1 also shows the locations of NWS upper-air sounding sites at Medford (MFR), Salem (SLE), and Quillayute (UIL) that released extra rawinsondes during some of the flights, boundary layer (915 MHz) wind profiler sites, and the P-3 base at Boeing Field (BFI) in Seattle, Washington.

The lack of sufficient routine coastal observations was addressed with a pair of field experiments using one of NOAA's P-3 research aircraft as the principal observing platform. The P-3 was ideally suited for collecting the necessary observations because of its logistical flexibility and its ability to both map mesoscale structures and sample small-scale phenomena such as boundary layer turbulence and cloud microphysical processes under relatively severe conditions. As described in Jorgensen et al. (1983), the P-3 gathers continuous in situ measurements of standard navigational and meteorological parameters at 1 Hz (and a subset of these at 40 Hz) and remote measurements of reflectivity and radial wind velocity from a helically scanning tail-mounted Doppler radar. The aircraft observations were supplemented by special surface-based instrumentation, including NOAA/Environmental Technology Laboratory's (ETL) 915-MHz boundary layer wind profilers at various locations along the Oregon and northern California coasts (see Rogers et al. 1993 for a description of performance characteristics), and by enhancements to the operational surface weather station network.

The overall experimental strategy was to operate the special surface-based instrumentation continuously and to task the P-3 for synoptic situations of special interest. These situations generally included strong low-level winds and significant precipitation, usually

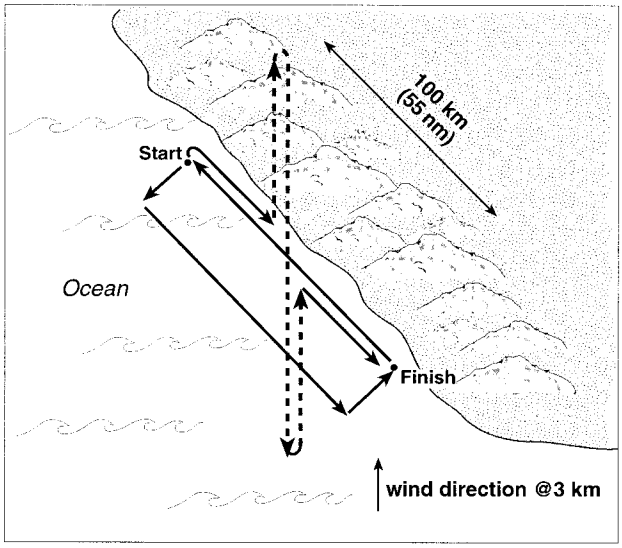

FIG. 2. Schematic of Doppler radar–cloud microphysical flight module designed for COAST. The solid (dotted) lines refer to the portion of the pattern focusing on Doppler radar (cloud microphysical) observations. The Doppler radar rectangle was generally oriented parallel to the coast or a precipitation feature and was flown at ~3000 m; the cloud microphysical legs were oriented parallel to the flow at ~3000 m and flown at the −4°, −8°, and −12°C levels.

in association with fronts or other spatially and temporally varying weather phenomena. The basic flight strategy was to map the low-level flow both offshore, well upstream of the terrain, and in the coastal zone, relying predominantly on the synthetic dual-Doppler radar capability of the P-3 (Jorgensen and Smull 1993). These radar measurements were accompanied by flight-level meteorological and cloud microphysical (liquid water content, and cloud and precipitation particle) observations, and vertical profiles from dropwindsondes.

The success of our field effort using the P-3 depended on being able to anticipate structures of interest with lead times of at least 24–36 h. On these timescales we relied heavily on the synoptic-scale predictions by operational NWP models for the eastern Pacific and West Coast. Their coarse resolution precludes an accurate description of the mesoscale flow in the coastal zone. The performance of these models on the synoptic scale ranged from fair to excellent; their systematic errors included a tendency to bring fronts and other features onshore too quickly. It is noteworthy that they predicted well the two most severe weather events of the field program (the strong southwesterlies of 9 December 1993 and the storm of 12 December 1995).

A basic flight pattern or module was designed to sample mesoscale coastal phenomena (Fig. 2). Its primary objectives were to document systematically and efficiently the evolution of the flow impinging upon coastal orography (largely through Doppler radar measurements) and the modification of ice microphysical and precipitation processes (principally through flight-level meteorological and cloud microphysical observations). Guiding principles included keeping the module relatively simple and short (~2 h of flight time) so it could be repeated. Our intent was to sample intensively a mesoscale segment (~100 km) of the coast rather than to survey a large region. As illustrated in Fig. 2, the module consisted of two main components: an elongated box situated on the upwind side of the coastal terrain with its long axis parallel to the terrain, and legs at generally the −4°, −8°, and −12°C levels, extending from offshore to over the terrain and oriented parallel to the flow at ~3 km altitude. The first component provided high quality Doppler radar observations; flying mostly parallel to features of interest (typically aligned along the vertical shear) helped reduce the ambiguity in unfolding velocities and hence helped resolve the cross-terrain or cross-band component of the flow. The second component focused on microphysical measurements, in particular the changes in ice habit during precipitation fallout. Our first priority was to repeat this module in the coastal zone, as the dynamical structure of interest approached the coast and made landfall; when precipitation was absent in the coastal zone, the module was flown relative to a propagating feature such as a rainband or front as it approached the coast. These modules were designed for regions of precipitation; when only direct flight-level measurements were possible, other types of maneuvers were executed.

Table 1 summarizes the flight operations during the first field phase in December 1993. More detail is provided on a selected subset of these cases in the following section. Weather conditions during the first field phase were favorably stormy (on four of the six flights, observed wind speeds below 1 km reached or exceeded 35 m s^{-1}), but the overall objective of sampling landfalling storms was not fully met. The strongest fronts of the experiment (the flights of 3 and 8 December) were well sampled in the offshore to nearshore domain but not over coastal terrain. Probably the most effective sampling in the coastal zone (the flight of 9 December) was conducted in a quasi-steady-state situation. These shortcomings, along with our success in sampling very interesting mesoscale structures, moti-

vated the second field phase in December 1995. Drawing upon our experience in 1993, notable changes were made in the organization of the second phase, including the availability of two flight crews, for logistical flexibility and the option of back-to-back flights, and the modification of the flight plans to execute simpler, repeated patterns, largely in the coastal zone. Table 2 summarizes the flights for December 1995. While the weather during 1995 was not as consistently stormy as during 1993, the quality of the data was high and some severe events were sampled. In particular, two missions were conducted into the severe wind storm of 12 December 1995.

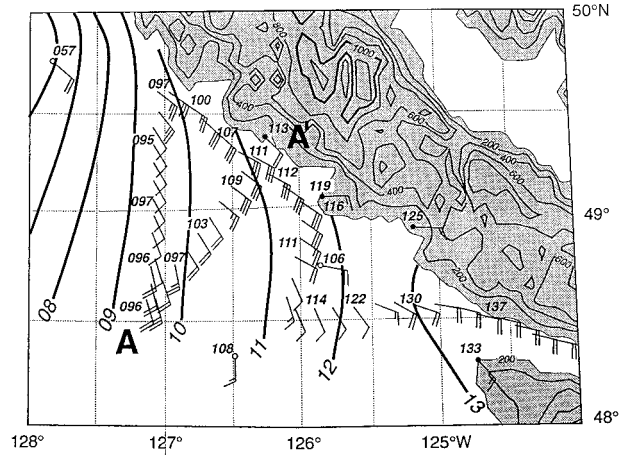

FIG. 3. Map of flight-level winds at approximately 100 m, surface reports over land and water (closed and open circles, respectively), and sea level pressure in mb (solid lines) for the case of 1 December 1993. Selected sea level pressures from aircraft height and pressure measurements are also indicated.

4. Highlights of individual cases

a. 1 December 1993: Coastally enhanced winds during moderate onshore flow

This case was included in the combined observational-scale analysis of Overland and Bond (1995) and is briefly summarized here. The objective of the flight of 1 December was to document flow along the west coast of Vancouver Island during moderate and relatively steady-state onshore-directed winds. The focus was on pressure and wind perturbations windward of the terrain.

A map of flight-level winds, sea level pressure, and surface reports (Fig. 3) reveals the ridging and enhanced alongshore flow that occurred in the coastal zone. A vertical cross section (Fig. 4) from a vertical stack flown normal to the coastline shows that the low-level flow along the coast was 2 K cooler and had an alongshore wind velocity 6 m s^{-1} greater than the undisturbed flow offshore. The horizontal and vertical extents of this trapped flow were about 40 km and 500 m, respectively.

The observed horizontal and vertical extents of the trapped flow were compared with values provided by a simple scale analysis based on the Froude number, $F = U/(hN)$, where U is the onshore velocity, h is a height scale, and N is the Brunt–Väisälä frequency. For conditions in which the mountain Froude number $F_m = U/(h_m N)$ is less than 1, where h_m is the terrain height, the scale height of the trapped flow can be less than the height of the terrain. Instead, the depth of the trapped flow is the inertial or gravity height scale determined by setting the Froude number of the flow equal to 1, that is, $h \sim U/N$. For the case of 1 December 1993, this height was ~500 m, in agreement with observations. The scaling also provides a horizontal scale for the offshore extent of the trapped flow. This scale is the Rossby radius $L = Nh/f$, where f is the Coriolis parameter and h is the observed or predicted height scale. The Rossby radius for the case of 1 December was ~50 km, in rea-

TABLE 1. COAST I flight summary, December 1993.

Date	Phenomenon	Topics/results
1*	Barrier jet; Vancouver Island	Height of coastal modification scales as *U/N*
3*	Intense, narrow cold front; offshore	Mesoscale character of front simulated by MM5
8	Intense, convective cold front; nearshore	Doppler analysis; validation of COAMPS
9*	Strong, SW flow; Olympics, Oregon coast	Observation and simulation of terrain-induced features
11*	Moderate NW flow; Olympics	Near-neutral stability, in contrast with 1 and 8 December
13	Vigorous cold front; Vancouver Island	Microscale frontal structure at coast versus offshore

*The asterisks indicate cases discussed in the next section.

TABLE 2. COAST II flight summary, 1995.

Date	Phenomenon	Possible topics
29 November	Southwesterly flow; northern Oregon	Rainband modification by modest 2D terrain
1 December*	Cold front; southern Oregon	Terrain effects on precipitation and frontal propagation
3 December	Cold, southwesterly flow; Olympics, Vancouver Island	Ice microphysics at –20°C; 3D vs 2D barrier
9 December	Warm front; Vancouver Island	Low-level modification of front; TKE distributions; gap winds
10 December	Strong southerlies; southern Oregon	Nearshore vs coastal winds; boundary layer wind profiles
11 December	Deep, maturing low; offshore Oregon	Open-ocean structure; mesoscale measurement strategies
12 December*	Landfalling low; Olympic Mtns.	Evolution of flow during landfall; coastal effects near wind maximum
17 December	Occluded front; Vancouver Island	Low-level damming; wake effects; rainband modification

*The asterisks indicate cases discussed in the next section.

sonable agreement with the observed seaward extent of the trapped flow. This particular case represented a relatively simple situation, with only minimal diabatic effects due to latent heating and a quasi-steady background flow. In general, nonconservative processes and temporal and spatial variations in the velocity and static stability of the incident flow will modify the orographic response and at least complicate, if not invalidate, simple scale analysis.

b. 3 December 1993: An intense, landfalling front

On 3 and 4 December 1993, a maritime cold front advanced toward and made landfall along the northwest coast of the United States. The thermodynamic, kinematic, and precipitation distributions in the vicinity of this front were documented through the analysis of offshore aircraft data, coastal wind-profiler data, and land- and ocean-based surface data at 1-h resolution (Neiman et al. 1995). A sea level pressure analysis at 1800 UTC 3 December 1993 (Fig. 5) shows a nearly north–south-oriented maritime cold front situated ~400–500 km west of Washington and Oregon. Rainbands with convective elements (not shown) paralleled the surface front at its leading edge; broader and more stratiform bands were present within the cold sector. The morphology and organization of these rainbands resembled the narrow and wide cold-frontal rainbands discussed by Houze (1991), among others. Using a cross-section analysis of flight-level potential temperature and the front-parallel wind component along line AA' in Fig. 5, Neiman et al. (1995) showed that the portion of the front below 850 mb was narrow (<1 km wide) and nearly vertical. Aloft, the front broadened into a baroclinic zone about 200 km wide and tilted northwestward. We focus here on the steep leading portion of the front below 850 mb.

Offshore flight-level observations and airborne radar clearly resolved the microscale (<~1 km) character of the steep leading edge of the front, while airborne dual-Doppler wind field and kinematic diagnostics highlighted the three-dimensional air motions, vorticity, and convergence of the frontal environment. The 1-Hz aircraft observations taken during a frontal pen-

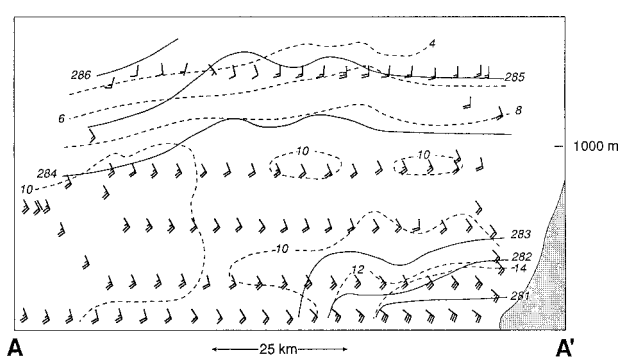

FIG. 4. Vertical cross section along the line AA′ of Fig. 3. The solid lines indicate potential temperature (K); the dashed lines indicate the along-barrier component of the wind (m s^{-1}) along 135°. Selected wind barbs are also shown. The terrain is indicated with shading.

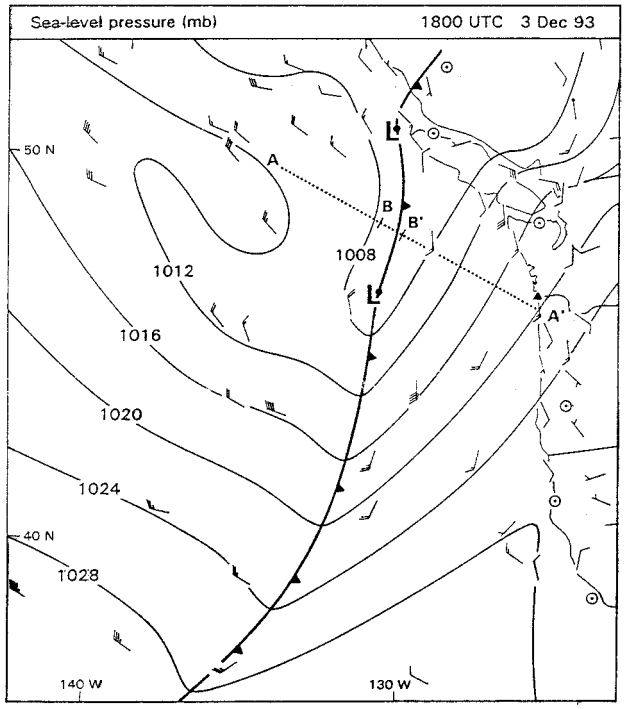

FIG. 5. Sea level pressure (mb) analysis at 1800 UTC 3 December 1993. Here AA′ and BB′ are projection lines for cross sections shown in Neiman et al. (1995). Wind vector flags = 25 m s^{-1}, barbs = 5 m s^{-1}, and half-barbs = 2.5 m s^{-1}. The Astoria wind profiler site is marked with a filled triangle. Analysis courtesy of C. Mass and M. Albright.

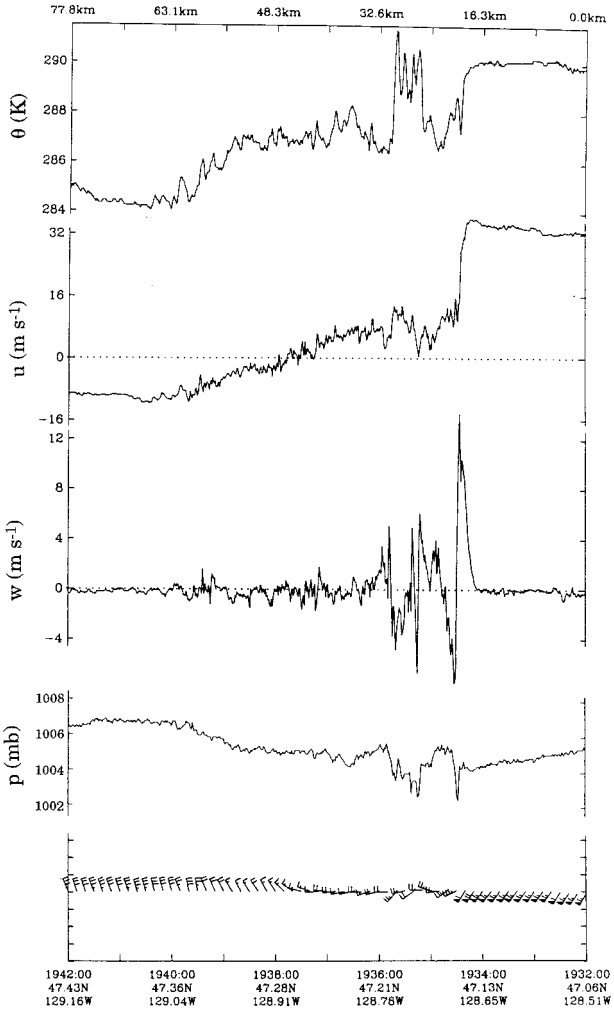

FIG. 6. NOAA WP-3D 1000-m above ground level flight-level traces with 1-s (~100 m) resolution for the period 1932–1942 UTC 3 December 1993 of potential temperature (K), the front-parallel wind speed (m s^{-1}), vertical velocity (m s^{-1}), sea level pressure (mb), and horizontal wind velocity vectors (as in Fig. 5; every tenth vector is shown). These observations were taken during a frontal transect in the vicinity of line BB′ in Fig. 4. Aircraft coordinates and corresponding times (UTC) are shown below the figure frame. Northwest is on the left side of the time series.

etration at 1000 m between about 1934 and 1938 UTC (Fig. 6) illustrate the large, rapid, and complex changes at the front when it was about 400 km offshore. A microscale frontal transition, encountered at ~1934:25 UTC, included a 3–4-K decrease in potential temperature, a 25-m s^{-1} decrease in the front-parallel component of the flow, and an updraft of >12 m s^{-1} followed immediately by a 6-m s^{-1} downdraft. This vertical-motion couplet suggests convection. The microscale transition was followed by a turbulent "wake" from about 1935 to 1936 UTC that included large fluctuations in potential temperature and vertical velocity. The magnitude and rapidity of the changes in temperature, pressure, and wind near the leading edge of the front resemble those described for density current flows (e.g., Simpson 1969, 1972) and those documented for other strong fronts (Carbone 1982; Shapiro et al. 1985, among others). Note also the more gradual cyclonic shift in the wind and drop in temperature from about 1936 to 1940 UTC. This region represented the portion of the front that appears not to have been significantly affected by scale-contraction processes.

As the front approached the coast, prefrontal stratiform precipitation developed (not shown), quite likely due to terrain effects. The NOAA/ETL's 915-MHz wind profiler at Astoria, Oregon, provided ~1.5-min resolution wind-velocity and spectral-moment profiles of the frontal transition and its associated microphysical precipitation signatures along the coast adjacent to steep topography. The profiler observed small-scale wind and precipitation features at the leading portion of the front (not shown) remarkably similar to those observed offshore (i.e., the profiler showed vertical and temporal transitions that were consistent with spatial structures analyzed offshore). Preliminary nested high-

resolution (20-, 6.6-, and 2.2-km grids) numerical simulations of this maritime front (not shown) compare favorably with the observations. Ongoing numerical research and additional observation analysis are being used to determine quantitatively the dynamical and physical processes that were responsible for the frontal-scale contraction, the multibanded postfrontal precipitation, and the modulation of the prefrontal air flow and associated stratiform precipitation by the steep coastal topography.

c. 9 December 1993: Interaction of low-level southwesterly flow with the Olympic Mountains

The primary goal of this mission was to provide detailed three-dimensional analyses of the flow and precipitation around the Olympic barrier during relatively steady south-southwesterly flow (see Colle and Mass 1996 for a detailed description of this case). Because of the lack of conventional data in the areas of high terrain, the P-3 aircraft was used to collect flight-level and radar data. To the authors' knowledge, this is the first case in which aircraft-based dual-Doppler winds have been retrieved over an orographic barrier.

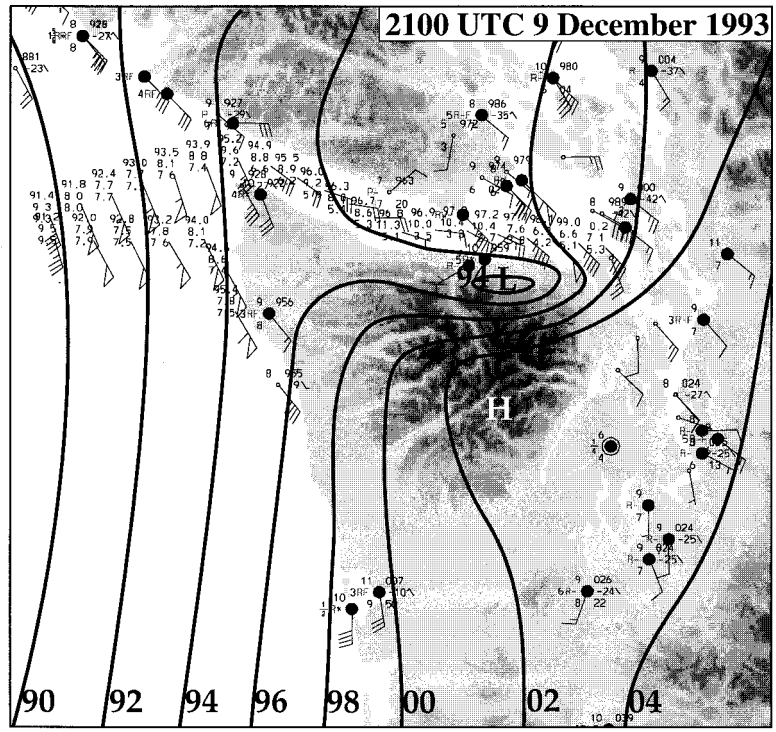

FIG. 7. Surface analysis at 2100 UTC 9 December 1993. Flight-level data from the NOAA P-3 at 150–200 m above the surface is plotted every 2 min between 2008 and 2130 UTC 9 December. The P-3 data for each point include sea level pressure (top), temperature in °C (middle), and dewpoint temperature in °C (bottom). The contour interval for sea level pressure is 2 mb. The symbol R* indicates rainfall of unknown intensity.

Figure 7 shows a surface analysis of the conventional synoptic data at 2100 UTC 9 December 1993 as well as flight-level data from the P-3 at ~150–200 m above the surface between 2008 and 2105 UTC. At this time, a deep occluded cyclone (minimum pressure of ~950 mb) was located southwest of British Columbia (not shown), which resulted in strong (25–40 m s^{-1}) low-level south-southwesterly flow impinging on the Olympics and well-defined pressure perturbations around the barrier. Lee troughing produced an enhanced pressure gradient on the northeast side of the Olympics, resulting in strong (~25 m s^{-1}) southeasterly flow to the south of the San Juan Islands (an archipelago in northern Puget Sound). In contrast, surface winds were nearly calm within the pressure ridging over the southeastern Olympics. Meanwhile, along the Washington coast the winds were mainly southeasterly at ~15–20 m s^{-1}. Flight-level winds show the rapid transition from strong southeasterly flow (25 m s^{-1})

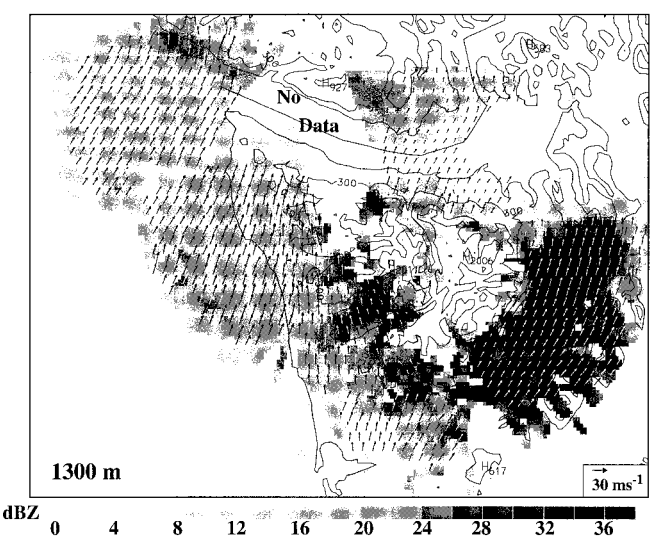

FIG. 8. NOAA P-3 Doppler winds and radar reflectivity factor (shaded) at 1300 m above mean sea level between 1900 and 2200 UTC 9 December 1993. Topography is contoured every 500 m, starting at 300 m.

over the Pacific to easterly flow (15 m s^{-1}) at the western entrance to the Strait of Juan de Fuca. These easterlies weakened to less than 5 m s^{-1} north of the Olympics, where the temperature reached a local maximum as a result of the strong downslope flow over the northern slopes of the Olympics.

As the P-3 circled the Olympic barrier between 1900 and 2200 UTC 9 December, interesting flow and precipitation structures were observed from the tail Doppler radar. At 1300 m above mean sea level (Fig. 8), flow splitting could be seen around the pressure ridging over the southern slopes of the Olympics. The winds were less than 10–20 m s^{-1} over the eastern Strait of Juan de Fuca, while stronger downslope flow (greater than 30 m s^{-1}) occurred on the north side of the Olympics. Enhanced radar reflectivity (greater than 30 dBZ) was situated over and immediately downwind of the ridges of the western Olympics as a result of forced ascent over the terrain and the subsequent advection of precipitation particles. Precipitation enhancement was also present along the windward side of Vancouver Island. In contrast, a rain shadow was present northeast of the Olympics.

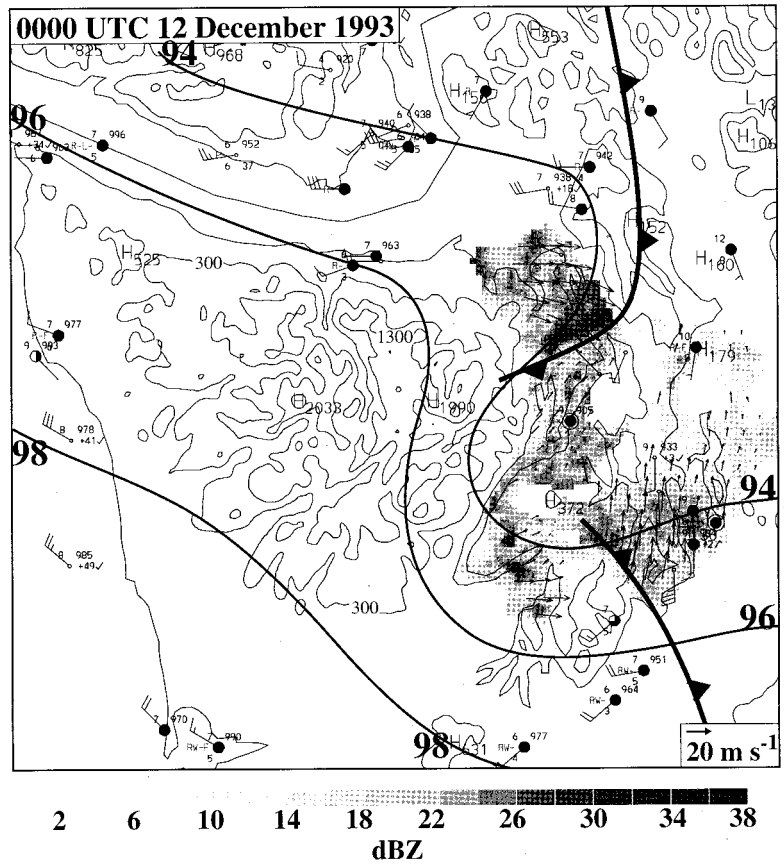

FIG. 9. Surface analysis at 0000 12 December 1993. NOAA P-3 Doppler winds and reflectivity (shaded) at 750 m above mean sea level between 2340 UTC 11 December and 0010 UTC 12 December 1993. The contour for sea level pressure is every 2 mb. The symbol R* indicates rainfall of unknown intensity.

This event was simulated at resolutions down to 3 km using the nonhydrostatic version of the Pennsylvania State–NCAR mesoscale model (MM5). As shown by Colle and Mass (1996), the model realistically simulated the observed wind and precipitation features around the Olympics. In addition, Colle and Mass showed that the asymmetry in the pressure pattern around the Olympics (lee troughing was 5–7 mb deeper than windward ridging) was a result of neither the asymmetry of the barrier itself (steeper lee slope) nor the reduction in the strength of the windward pressure ridge by latent heating. Instead, high stability near crest level and negative vertical wind shear above the barrier amplified the leeside mountain wave, which forced strong downslope flow and the pressure asymmetry. High-resolution model output was also used to determine some of the momentum balances around the barrier. Overall, this study has demonstrated the value of using a Doppler radar-equipped aircraft for studying flow and precipitation around orography. In addition, this research has shown the great potential of current mesoscale models for realistically simulating air flow and precipitation around mesoscale orographic barriers such as the Olympics.

d. 11 December 1993: Frontal interaction with the Olympic Mountains and a Puget Sound convergence zone

During COAST IOP 5, which occurred between 2000 UTC 11 December and 0200 UTC 12 December 1993, a cyclone and attendant fronts moved northeastward across the Olympic Peninsula, followed by offshore low-level ridging. As a result, this case provided an excellent opportunity to study the flow and precipitation evolution associated with cyclone/frontal passage across coastal orography, including the subsequent development of a Puget Sound convergence zone (Mass 1981).

Figure 9 shows a surface analysis of conventional synoptic data at 0000 UTC 12 December 1993 as well as Doppler winds and reflectivity data at 500 m above

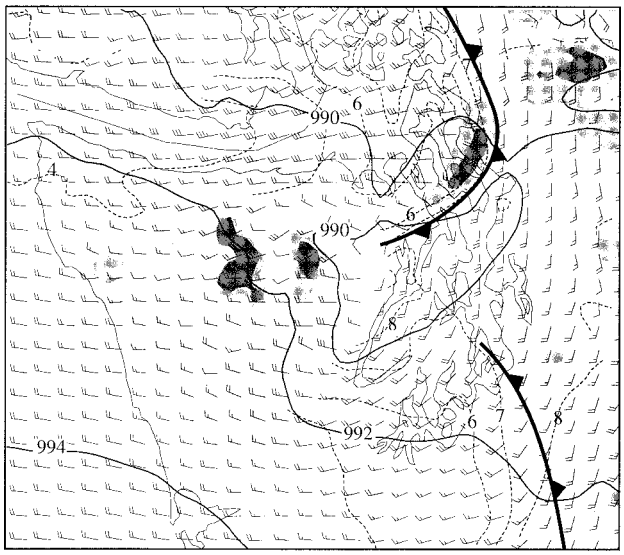

FIG. 10. Model analysis for a portion of the 3-km domain at 2300 UTC December 1993 (23 h) showing sea level pressure (solid line every 2 mb), winds (full barb = 10 kts) ~40 m above the surface, and temperatures (dashed line every 1°C) at 500 m MSL. The light, medium, and dark gray shading represents thresholds of precipitation mixing ratio (rain, snow, and graupel) of 0.04, 0.24, and 0.4 g kg^{-1}, respectively, at ~40 m above the surface.

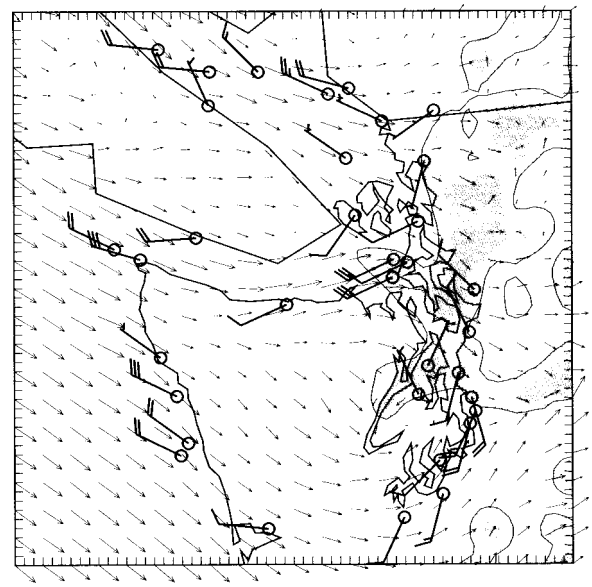

FIG. 11. Model-simulated 10-m wind vectors at 0100 UTC 12 December 1993 from a 13-h forecast from NRL's COAMPS model. The model-simulated 900-mb radar reflectivity between 20 and 30 dB*Z* is shown by the light shading and between 30 and 40 dB*Z* by the darker shading. Surface wind observations are plotted with one full wind barb corresponding to 10 m s^{-1}.

mean sea level from the NOAA P-3 between 2330 UTC 11 December and 0000 UTC 12 December 1993. A cold front extending southward over western Washington was distorted over Puget Sound as a result of low-level flow splitting around the Olympics. One segment of the front was moving eastward across southern Puget Sound while the other pushed southeastward around the northeast corner of the Olympics. Associated with the northern section of the front was a rapid wind shift from southwesterly to strong westnorthwesterly flow (~20 m s^{-1}) and surface temperature drops of 2°–3°C. The largest reflectivities (>30 dB*Z*) at 500 m were located immediately behind this 500-m wind shift region, and a region of mainly stratiform precipitation (25–30 dB*Z*) extended to the northwest of the front. Meanwhile, the front over southern Puget Sound had primarily a northwest–southeast orientation. The surface temperatures decreased ~2°C across this portion of the front, and the low-level winds veered from southerly to southwesterly. During the next 2 h, the northern portion of the front pushed southward and became stationary across central Puget Sound, resulting in a classic convergence zone structure (a nearly east–west band of precipitation and surface easterlies across central Puget Sound).

This event was simulated down to 3-km resolution using the MM5 model. The simulated front was approximately an hour fast; therefore, Fig. 10 shows the 3-km model analysis at 2300 UTC 11 December (23 h into the forecast). Overall, the low-level structures are similar to the structures observed in the lee of the Olympics, including the enhanced precipitation immediately behind the frontal transition over northern Puget Sound.

This case has also been simulated using a high-resolution (Δx = 5 km) version of COAMPS (Hodur 1997). Figure 11 shows the 10-m wind vectors at 13 h (0100 UTC 12 December) associated with the aforementioned Puget Sound convergence zone, in reasonable agreement with the observations. The model-simulated radar reflectivity also corresponds well with the precipitation observed with the convergence zone. Future plans include detailed model comparisons between COAMPS and MM5. These comparisons will facilitate greater understanding of model capabilities and deficiencies, and will guide improvements in data assimilation and initialization techniques.

e. 1 December 1995: Landfall of a cold-frontal rainband along the southern Oregon coast

This mission captured the development and landfall of a cold-frontal rainband and accompanying

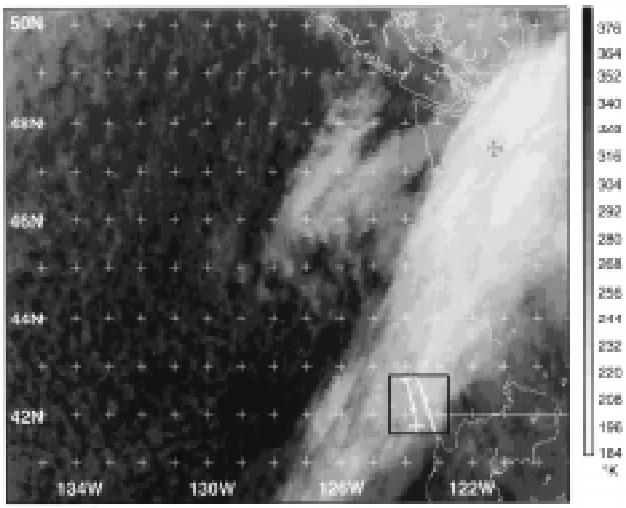

FIG. 12. Mission summary of IR satellite imagery from *GOES-7* (temperature indicated by the table on the right) and NOAA P-3 flight track for 0635 UTC 1 December 1995.

heavy prefrontal precipitation along the southern Oregon–northern California coast on 1 December 1995. While this event was not particularly severe, it offers a well-documented example of frontal interaction with a relatively two-dimensional segment of steep coastal terrain. A unique aspect of this case is that both flight modules were executed within the region being scanned by National Weather Service WSR-88D Doppler radar located near Eureka, California (BHX, cf. Fig. 1), and by a research wind profiler operated by NOAA/ETL at Crescent City, California (CEC, cf. Fig. 1).

During its initial low-level survey (Fig. 12), the aircraft encountered a developing band of precipitation approaching the southern Oregon coast (Fig. 13a). This band included a broken line of cellular precipitation extending southwestward of the southern Oregon coast in a region of southwesterly flow at 1 km above mean sea level (MSL) with modest cyclonic shear but little change in wind direction. Just 1.5 h later, however, profound changes were evident. A strong wind shift from southwesterly to westerly flow extending to the 1-km level suggests frontogenesis (Fig. 13b). The accompanying reflectivity pattern evinces two distinct types of precipitation enhancement: (1) a narrow but locally intense northeast–southwest narrow cold-frontal rainband (Houze et al. 1976) coincident with the wind shift and (2) a broader shield of precipitation upwind and oriented parallel to the steep coastal terrain, with embedded cellular cores of heavier precipitation along and just inland of the coast. The most intense reflectivity values (40–50 dB*Z*) occurred at the intersection of these two features.

The P-3 completed two Doppler–microphysical modules in the vicinity of this intensifying band where it intersected the steep coastal topography. Microphysical data (not shown) were collected up to –8°C in the first module, and to –12°C during the second module. During the P-3's final northbound leg (~1000–1030 UTC, not shown), the aircraft passed through a weaker trailing rainband marked by substantial clearing and pronounced drying (dewpoints < –25°C at a flight level of 3000 m), consistent with deep subsidence in the wake of the advancing cold front.

The MM5 was used to simulate this IOP down to 3-km resolution in order to diagnose the complex terrain–frontal interactions. Figure 14 shows the model output 17 and 19 h into the simulation (1500 and 1700 UTC December 1995, respectively). Overall, the structural evolution is qualitatively similar to that observed with the NOAA P-3 aircraft (Fig. 13). At 0500 UTC (Fig. 14a), a broken line of precipitation extended southwestward of the southern Oregon coast in a region of weak low-level baroclinicity and horizontal shear. By 0700 UTC (Fig. 14b), this tempera-

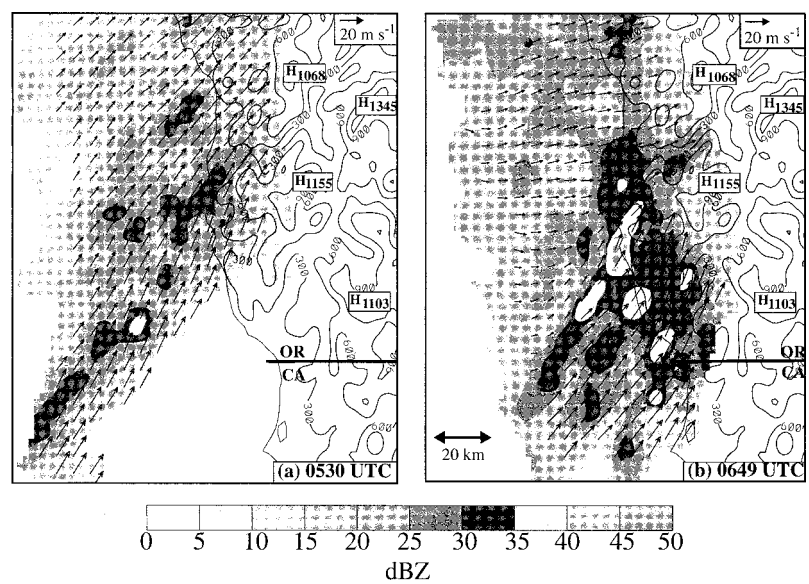

FIG. 13. Horizontal cross section of radar reflectivity (dBZ; indicated by the gray scale on the bottom) and horizontal wind velocity at 1 km MSL for (a) 0530 and (b) 0649 UTC 1 December 1995.

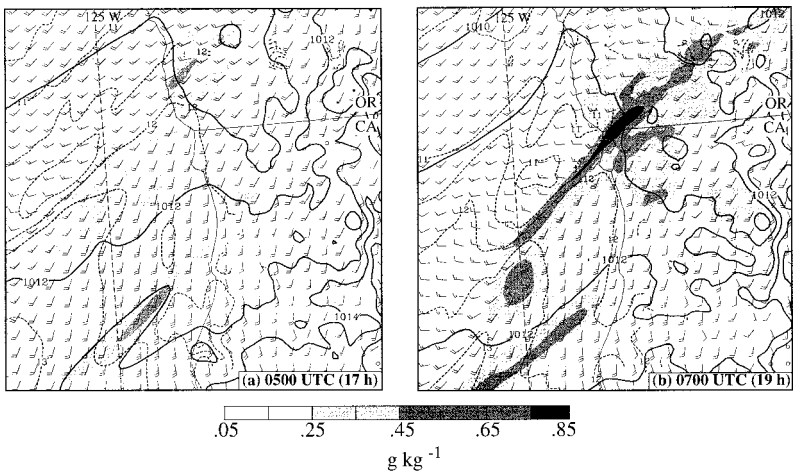

FIG. 14. MM5 numerical model results from the innermost computational domain (3-km horizontal resolution) valid at (a) 0500 and (b) 0700 UTC 1 December 1995 (17 and 19 h into the simulation, respectively). Fields shown are near-surface ground-relative winds (~40 m above the surface, full barb = 10 kt), sea level pressure (solid contours every 1 mb), temperature at 0.5 km MSL (dashed contours, every 0.5°C), and precipitation mixing ratio at ~40 km MSL (g kg^{-1}, shading key on bottom).

ture gradient and precipitation band had intensified, with the maximum precipitation mixing ratios located slightly inland at the intersection of the frontal and orographic lifting zones, as observed. Some minor failings of the simulation are that this intense precipitation band is shifted ~30 km southward of its observed position, and the southwesterlies to the north of this band are not supported by the available observations.

f. 11–12 December 1995: Offshore and coastal structure of a deep cyclone

The storm of 11–12 December 1995 caused five fatalities and over $200 million in damage along the U.S. west coast (NCDC 1995). We believe there is substantial interest in this event among both the operational and research communities. Because our work on this case is in its early stages, the material included here is intended largely as a prelude to further research.

Observations by the P-3 along the Oregon coast during the second flight into this storm illustrate its severity. Figure 15 shows selected flight-level winds measured by the P-3 between about 1930 and 2130 UTC 12 December during "porpoising" between altitudes of about 600 and 1400 m. Most of this region lacked precipitation during the time of this survey, and thus only directly measured winds are generally available. There were observations of temperature and wind fluctuations at 40 Hz, which are being used to characterize the turbulence during this high-wind situation. The P-3 found a wind speed maximum of ~49 m s^{-1} at ~1200 m during the leg flown about 100 km offshore; the corresponding maximum speed was ~46 m s^{-1} on the following leg about 10 km offshore. Surface stations along the central Oregon coast were reporting peak sustained winds of ~30 m s^{-1} and maximum gusts

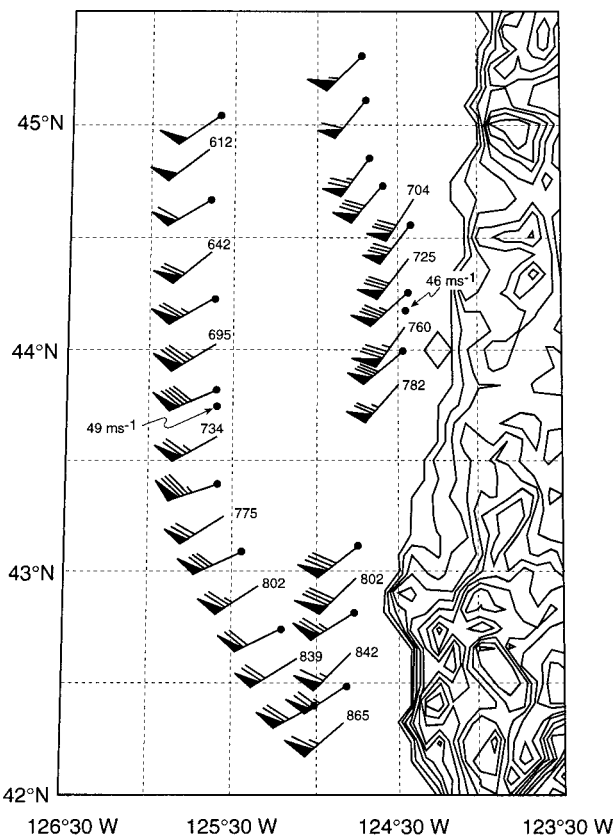

FIG. 15. Selected flight-level observations by the NOAA P-3 collected between 1928 and 2129 UTC 12 December 1995. The plotted winds represent 10-s averages (~1 km in horizontal extent) using the standard convention (flag = 25 m s^{-1}; each full barb = 5 m s^{-1}). The winds at the lowest level flown (~600 m) are accompanied by the sea level pressure plotted in the standard convention. The winds at the highest altitude flown (~1400 m) are indicated by a large dot. The maximum 10-s winds encountered on the offshore and near coastal legs are also indicated. The solid contours represent the terrain coarsely at 100-m intervals.

exceeding 50 m s^{-1}. There appears to have been only slight orographic modification of the flow in the coastal zone, at least at flight level. The wind direction was somewhat more southerly along the coast than farther offshore; this may not have been terrain induced, but rather a consequence of curvature in the flow inherent to the storm. A large orographic response would not be expected upstream of the terrain in this situation, since the terrain (envelope height ~700 m) and static stability ($N \sim 8 \times 10^{-3}$ s^{-1}) were modest, and the onshore velocity ($U \sim 15$–20 m s^{-1}) was substantial, so the Froude number (Fr ~ 3) was large. The numerical studies of this aspect of the storm will focus on the boundary layer structure, for example, whether the simulations reproduce the low-level profiles of wind and turbulence observed by the aircraft, and on the modification of the boundary layer by the coastal terrain.

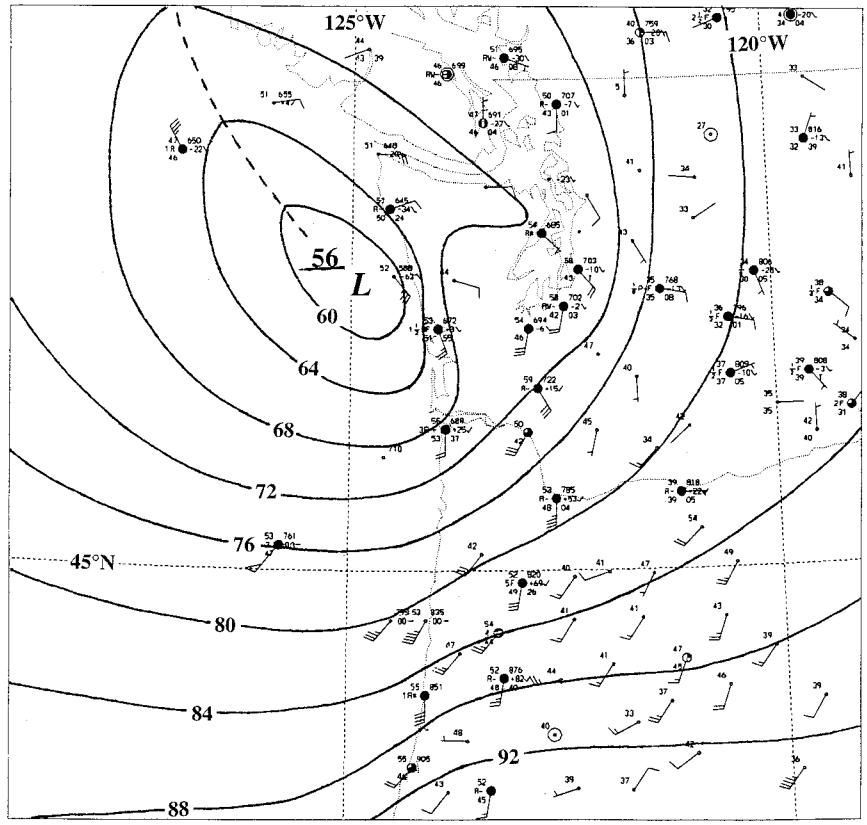

FIG. 16. Preliminary sea level pressure analysis (contour interval 4 mb) for 0000 UTC 13 December 1995. Many of the observations over the land are omitted for clarity.

Synoptic conditions for the latter portion of the second flight are summarized with a mesoscale sea level pressure analysis for 0000 UTC 13 December (Fig. 16). This analysis is preliminary; high-resolution model runs will be used to help identify and track mesoscale features such as fronts and troughs in this complex and evolving synoptic situation. Figure 16 shows a 956-mb low situated about 50 km off the coast of Washington. An intense pressure gradient was present along the Washington coast east of the center, presumably due in part to windward ridging along the Olympic Mountains. Given this gradient, the surface winds were modest (up to about 17 m s^{-1}) and hence clearly subgeostrophic. The surface winds along the Oregon coast were generally stronger (with sustained magnitudes up to 23 m s^{-1}) even though the pressure gradient was weaker.

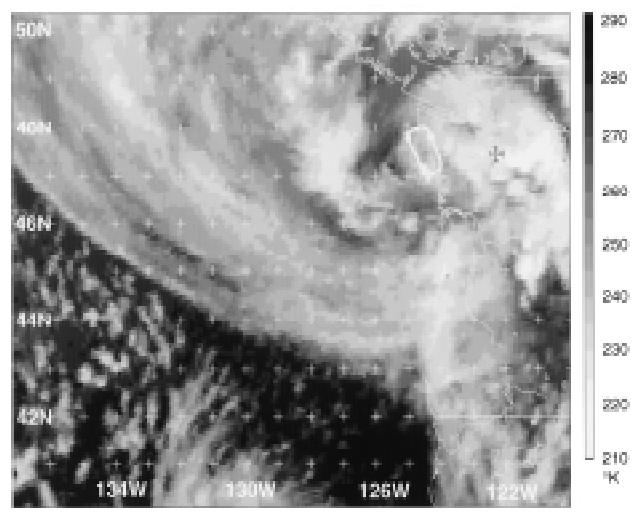

FIG. 17. Infrared satellite image for 2336 UTC 12 December 1995 from *GOES-7* overlain by a portion of a flight module (see Fig. 2) being executed at this time.

The P-3 executed Doppler radar–cloud microphysical surveys in the coastal region along the western flank of the Olympic Mountains from about 2200 to 0200 UTC as the low approached. Figure 17 shows an infrared satellite image for 2336 UTC overlaid by a segment of one of the flight modules executed at that time. The satellite image suggests that the center of the circulation was near the coast (as indicated by Fig. 16) and that perhaps a back-bent occlusion similar to that discussed by Steenburgh and Mass (1996) was poised

about 150 km offshore. Precipitation covered the coastal zone and Olympic Mountains, and it appears that a complete and high quality dataset of Doppler radar data was collected by the aircraft in this region. The analysis of this data is in progress; we expect some very interesting results given the prominence of the terrain and the intensity of the storm.

5. Final remarks

This article on the COAST program has shown the direction of its research on the orographic modification of landfalling storms and has illustrated its recent field activities. The measurements collected by a NOAA P-3 research aircraft and ancillary coastal observations provided unique datasets. These datasets have been used both to examine directly the structure and dynamics of a variety of mesoscale coastal features and to serve as sources of verification for high-resolution numerical model simulations. Initial comparisons of these simulations with the detailed measurements from COAST indicate that the models can realistically duplicate mesoscale structures in complex coastal terrain when the synoptic-scale flow is well defined. It bears emphasizing that most of the work is in progress; more observational/modeling case studies from COAST may be expected in the near future.

COAST has focused on the U.S. west coast, but its results are directly applicable to other regions with similar terrain and synoptic forcing, such as the coastal zones of Alaska, Norway, Chile, and New Zealand. And since the phenomena studied by COAST are not restricted to coastal zones, just about any midlatitude region with prominent orographic relief will experience some of the same type of storm–terrain interactions.

The monitoring of coastal weather in the United States and some other parts of the world is being improved, principally through advances in remote sensing of winds and precipitation via Doppler radar and satellite. But improvements in forecasting also require better understanding and prediction of the evolution of coastal zone weather, which will increasingly rely upon output from high-resolution NWP models. Results from COAST are contributing to the evaluation and improvement of such models.

Acknowledgments. We wish to recognize the role of ONR's Coastal Meteorology ARI, under the direction of Gary Geernaert, Tom Kinder, and Scott Sandgathe, for its support of the field work and many of the principal investigators. We extend special thanks to NOAA's Aircraft Operations Center, notably Cmdr. Phil Kennedy and program manager Jack Parrish, for the successful execution of flight operations under frequently adverse conditions. Finally, we acknowledge all the other individuals associated with COAST (notably those from the University of Washington, the NWS Forecast Offices in Seattle and Portland, and NOAA/ETL) for their essential assistance in both field and other operations.

References

Bell, G. D., and L. F. Bosart, 1988: Appalachian cold-air damming. *Mon. Wea. Rev.*, **116**, 137–161.

Blumen, W., 1992: Propagation of fronts and frontogenesis versus frontolysis over orography. *Meteor. Atmos. Phys.*, **48**, 37–50.

Carbone, R. E., 1982: A severe frontal rainband. Part I: Stormwide hydrodynamic structure. *J. Atmos. Sci.*, **39**, 258–279.

Colle, B., and C. F. Mass, 1996: An observational and modeling study of the interaction of low-level southwesterly flow with the Olympic Mountains during COAST IOP 4. *Mon. Wea. Rev.*, **124**, 2152–2175.

Grell, E. D., and M. A. Shapiro, 1994: Visualization of the life cycle of a rapidly intensifying oceanic cyclone. *Life Cycles of Extratropical Cyclones: An International Symposium,* Vol. II, Bergen, Norway, The Norwegian Geophysical Society and the American Meteorological Society, 202–207.

Gross, B. D., 1994: Frontal interaction with isolated orography. *J. Atmos. Sci.*, **51**, 1480–1496.

Hodur, R. M., 1997: The Naval Research Laboratory's Coupled Ocean Atmosphere Mesoscale Prediction System (COAMPS). *Mon Wea. Rev.*, **125,** 1414–1430.

Hoinka, K. P., M. Hagen, H. Volkert, and D. Heimann, 1990: On the influence of the Alps on a cold front. *Tellus*, **42A,** 140–164.

Houze, R. A., Jr., 1991: *Cloud Dynamics.* Academic Press, 573 pp.

——, J. D. Locatelli, and P. V. Hobbs, 1976: Dynamics and cloud microphysics of the rainbands in an occluded frontal system. *J. Atmos. Sci.*, **33,** 1921–1936.

Jorgensen, D. P., and B. F. Smull, 1993: Mesovortex circulations seen by airborne Doppler radar within a bow-echo mesoscale convective system. *Bull. Amer. Meteor. Soc.*, **74,** 2146–2157.

——, P. H. Hildebrand, and C. L. Frush, 1983: Feasibility test of an airborne pulse-Doppler meteorological radar. *J. Climate Appl. Meteor.*, **22,** 744–757.

Kuo, Y.-H., M. A. Shapiro, and E. G. Donall, 1991: The interaction between baroclinic and diabatic processes in a numerical simulation of a rapidly intensifying extratropical marine cyclone. *Mon. Wea. Rev.*, **119,** 368–384.

Mass, C. F., 1981: Topographically forced convergence in western Washington State. *Mon. Wea. Rev.*, **109,** 1335–1347.

——, and G. K. Ferber, 1990: Surface pressure perturbations produced by an isolated mesoscale topographic barrier. Part I: General characteristics and dynamics. *Mon. Wea. Rev.*, **118,** 2579–2596.

NCDC, 1995: *Storm Data*, **37** (12), 111 pp. [Available from National Climatic Data Center, 151 Patton Ave., Asheville, NC 28801.]

Neiman, P. J., and M. A. Shapiro, 1993: The life cycle of an extratropical marine cyclone. Part I: Frontal-cyclone evolution and thermodynamic air–sea interaction. *Mon. Wea. Rev.*, **121,** 2153–2176.

——, ——, and L. S. Fedor, 1993: The life cycle of an extratropical marine cyclone. Part II: Mesoscale structure and diagnostics. *Mon. Wea. Rev.*, **121,** 2177–2199.

——, ——, B. F. Smull, and D. Johnson, 1995: A comparison of offshore observations and coastal wind profiler observations during a land-falling frontal system adjacent to steep topography. Preprints, *Seventh Conf. on Mountain Meteorology*, Breckenridge, CO, Amer. Meteor. Soc., 245–250.

Okland, H., 1990: The dynamics of coastal troughs and coastal fronts. *Tellus*, **42A,** 444–462.

Overland, J. E., and N. A. Bond, 1993: The influence of coastal orography: The Yakutat storm. *Mon. Wea. Rev.*, **121,** 1388–1397.

——, and ——, 1995: Observations and scale analysis of coastal wind jets. *Mon. Wea. Rev.*, **123,** 2934–2941.

Parish, T. R., 1982: Barrier winds along the Sierra Nevada mountains. *J. Appl. Meteor.*, **21,** 925–930.

Parsons, D. B., and P. V. Hobbs, 1983: The mesoscale and microscale structure and organization of clouds and precipitation in midlatitude cyclones. IX: Some effects of orography on rainbands. *J. Atmos. Sci.*, **40,** 1930–1949.

Pierrehumbert, R. T., and B. Wyman, 1985: Upstream effects of mesoscale mountains. *J. Atmos. Sci.*, **42,** 977–1003.

Rogers, R. R., W. L. Ecklund, D. A. Carter, K. S. Gage, and S. A. Ethier, 1993: Research applications of a boundary-layer wind profiler. *Bull. Amer. Meteor. Soc.*, **74,** 567–580.

Rotunno, R., and Coauthors, 1996: Coastal meteorology and oceanography: Report of the third prospectus development team of the U.S. Weather Research Program to NOAA and NSF. *Bull. Amer. Meteor. Soc.*, **77,** 1578–1585.

Shapiro, M. A., T. Hampel, D. Rotzoll, and F. Mosher, 1985: The frontal hydraulic head: A micro-α scale (~1 km) triggering mechanism for mesoconvective weather systems. *Mon. Wea. Rev.*, **113,** 1166–1183.

Simpson, J. E., 1969: A comparison between laboratory and atmospheric density currents. *Quart. J. Roy. Meteor. Soc.*, **95,** 758–765.

——, 1972: Effects of the lower boundary on the head of a gravity current. *J. Fluid Mech.*, **53,** 759–768.

Smith, R. B., 1981: An alternative explanation for the destruction of the Hood Canal bridge. *Bull. Amer. Meteor. Soc.*, **62,** 1319–1320.

Smolarkiewicz, P. K., and R. Romnno, 1989: Low Froude number flow past three-dimensional obstacles. Part I: Baroclinically generated lee vortices. *J. Atmos. Sci.*, **46,** 1154–1164.

Steenburgh, W. J., and C. F. Mass, 1996: Interaction of an intense extratropical cyclone with coastal orography. *Mon. Wea. Rev.*, **124,** 1329–1352.

Williams, R. T., M. S. Peng, and D. A. Zankofski, 1992: Effects of topography on fronts. *J. Atmos. Sci.*, **49,** 287–305.

Xu, Q., 1990: A theoretical study of cold air damming. *J. Atmos. Sci.*, **47,** 2969–2985.